Published as: *Nature*. 2013 October 31; 502(7473): 703–706.

Meiotic chromosome structures constrain and respond to designation of crossover sites

Diana E. Libuda[1], **Satoru Uzawa**[3], **Barbara J. Meyer**[3], and **Anne M. Villeneuve**[1,2,*]

[1]Department of Developmental Biology Stanford University School of Medicine, Stanford, CA 94305, USA.

[2]Department of Genetics Stanford University School of Medicine, Stanford, CA 94305, USA.

[3]Howard Hughes Medical Institute and Department of Molecular and Cell Biology University of California at Berkeley, Berkeley, CA 94720, USA.

Abstract

Crossover (CO) recombination events between homologous chromosomes are required to form chiasmata, temporary connections between homologs that ensure their proper segregation at meiosis I[1]. Despite this requirement for COs and an excess of the double-strand DNA breaks (DSBs) that are the initiating events for meiotic recombination, most organisms make very few COs per chromosome pair[2]. Moreover, COs tend to inhibit the formation of other COs nearby on the same chromosome pair, a poorly understood phenomenon known as CO interference[3,4]. Here we show that the synaptonemal complex (SC), a meiosis-specific structure that assembles between aligned homologous chromosomes, both constrains and is altered by CO recombination events. Utilizing a cytological marker of CO sites in *Caenorhabditis elegans*[5], we demonstrate that partial depletion of the SC central region proteins (SYPs) attenuates CO interference, elevating COs and reducing the effective distance over which interference operates, indicating that SYPs limit COs. Moreover, we show that COs are associated with a local 0.4-0.5 μm increase in chromosome axis length. We propose that meiotic CO regulation operates as a self-limiting system in which meiotic chromosome structures establish an environment that promotes CO formation, which in turn alters chromosome structure to inhibit other COs at additional sites.

Although COs mature in the context of assembled SCs, whether the SC functions in CO interference has long been debated[6-8]. Based largely on analysis in budding yeast, it has been argued for the last decade that the SC is irrelevant for interference[6]. Consequently,

---

Correspondence and requests for materials should be addressed to A.M.V. (annev@stanford.edu).. *Correspondence to: annev@stanford.edu.

Supplementary Information is linked to the online version of the paper at www.nature.com/nature.

Author Contributions. D.E.L. and A.M.V. conceived and designed the experiments, analyzed the data, and wrote the paper. D.E.L. performed the experiments. S.U. deconvolved confocal images. S.U. and B.J.M. provided scientific discussions and technical expertise for computational straightening of chromosomes.

The authors declare no competing financial interests.

suggestive evidence that the SC might be involved in interference in other organisms has gained little traction[9,10]. The debate persists in part because of inherent limitations of some assays used to score COs (see discussion in Supplementary Information). We overcome this problem by taking advantage of the fact that the *C. elegans* CO-promoting protein COSA-1, which forms foci at nascent CO sites *in vivo*, serves as a robust cytological marker of the COs that elicit and respond to CO interference[5].

C. elegans exhibits robust CO interference, with chromosome pairs normally undergoing only a single CO[2]. Utilizing COSA-1 foci, we assessed whether SYPs function in limiting the number of COs per chromosome pair. SYPs are essential for CO formation[11-13], precluding use of *syp* null mutants for this analysis. To circumvent this issue, we used RNAi to partially deplete SYP-1 protein levels by ~60-70% (Extended Data Figure 1). In contrast to a prior study[9], the residual SYP-1 levels achieved using our experimental conditions were sufficient to permit assembly of SCs (albeit with reduced ratios of SYPs to axis subunits) and formation of chiasmata for all six chromosome pairs in most gonads (see Supplementary Discussion and Methods). Although SYPs are required to form COs, we found that partial depletion of SYP-1, SYP-2, or SYP-3 increases COSA-1 foci (Figure 1a; Extended Data Figure 2), indicating that a sufficient pool of SYPs is required to limit COSA-1-marked COs to one per chromosome pair.

In principle, an increase in COSA-1-marked CO sites could reflect an increase in the number of DSBs formed and/or an increase in the fraction of DSBs repaired as COs. Therefore, we controlled DSB number by using γ-irradiation to induce DSBs in *spo-11* mutant worms, which are proficient for pairing and SC assembly but lack endogenous meiotic DSBs (Figure 1b)[14]. Controls recapitulated the previous finding that increasing DSBs beyond the level needed to ensure at least one per chromosome pair (1000 Rad, 23.5 DSBs/nucleus) did not increase the average number of COSA-1 foci per nucleus beyond six[5]. Further, COSA-1 foci exhibited very low standard deviations (±0.14-0.27), reflecting operation of the robust CO control system. In contrast, upon *syp-1* RNAi, most nuclei exposed to >1000 Rad of γ-irradiation had >6 COSA-1 foci and standard deviations were much higher (±1.2-1.6), indicating impairment of CO control. This experiment demonstrates that increased DSBs alone cannot account for the increase in COSA-1 foci following SYP-1 partial depletion, and that for any given level of DSBs, SYP-1 plays a role in determining the fraction that will mature into cytologically-differentiated COs.

Our data suggest that SYP-1 partial depletion impairs CO interference. To investigate this further, we used worms homozygous for the two-chromosome fusion *mnT12* (X chromosome fused with chromosome IV)[10,15]. Previous work showed that while CO interference limits the *mnT12* chromosome pair to a single COSA-1 focus in the majority of meioses, *mnT12* chromosome pairs with two COSA-1 foci also occur[5]. Under our control conditions, 51% of *mnT12* pairs had a single COSA-1 focus, while 49% had two foci (Figure 2a-b; Methods). This occurrence of two COSA-1 foci along *mnT12* allowed us to assess interference strength in the context of wild-type SYP-1 levels and compare it to CO/chiasma interference in the context of SYP-1 partial depletion (Figures 1c, 2-4).

Increased COSA-1 foci following *syp-1* RNAi correlated with an increased number of cytologically-resolvable chiasmata on *mnT12* bivalents at diakinesis, the last stage of prophase (Figure 1c; Extended Data Figure 3). Consistent with *mnT12* having only one or two COSA-1 foci at the late pachytene stage in controls (average of 1.49 COSA-1 foci/ *mnT12* pair), control *mnT12* diakinesis bivalents had only one or two chiasmata. Upon *syp-1* RNAi, an average of 2.57 COSA-1 foci/*mnT12* pair were observed at late pachytene (49% having >3 foci; Figure 2b), and 47% of diakinesis bivalents had >3 chiasmata. These and other data (Extended Data Figure 3) indicate that the extra COSA-1 foci in *syp-1* RNAi worms represent *bona fide* cytologically-differentiated inter-homolog COs.

We conducted quantitative analyses evaluating the positions, distributions, and distances between COSA-1-marked sites on computationally straightened *mnT12* chromosomes (with HTP-3 immunofluorescence marking chromosome axes[16]; and, immunofluorescence for the HIM-8 protein, which localizes near the left end of the X chromosome[17], serving as an orientation marker) (Figure 2a; Methods). The average distance between COSA-1 foci on *mnT12* with ≥2 COSA-1 foci in *syp-1* RNAi was 4.5 μm, substantially shorter than the average distance of 8.5 μm for control *mnT12* with 2 foci ($p<0.0001$). Further, even when only *syp-1* RNAi *mnT12* with 2 foci were considered, the average distance (6.5 μm) was still significantly shorter than in controls ($p<0.0001$; Figure 2c). These data demonstrate that *syp-1* RNAi decreases the effective distance over which interference operates. The average distance between COSA-1 foci on control *mnT12* (8.5 μm) exceeds the average axis length of unfused autosomes (6.4 μm, $p<0.0001$), reinforcing the indirect inference of Hillers and Villeneuve[10] that interference in *C. elegans* operates over distances longer than the length of a normal chromosome.

We further assessed CO interference by dividing the *mnT12* axis into 8 evenly-spaced intervals and binning the positions of COSA-1 foci into these intervals (Figure 2d-e, Extended Data Figure 4). First, we compared the distributions of COSA-1 foci among these intervals for chromosomes with different numbers of foci. In controls, COSA-1 foci exhibited a specific non-random distribution indicative of interference: for the subset of chromosomes with only 1 COSA-1 focus, the single focus usually occurred near the middle of *mnT12*, whereas for the subset of chromosomes with 2 COSA-1 foci, those foci predominantly occurred near the chromosome ends (Figure 2d). In contrast, *syp-1* RNAi resulted in a fairly even distribution of foci along *mnT12*, regardless of the number of COSA-1 foci, consistent with attenuation of CO interference. Second, plotting the separation between adjacent pairs of COSA-1 foci (Figure 2e) revealed wide spacing (≥4 interval boundaries) separating adjacent COSA-1 foci in controls, and reduced separation between adjacent foci in *syp-1* RNAi worms, both when all pairs of foci or only chromosomes with 2 foci were considered.

We also used two quantitative methods to calculate interference strength. First, we performed a coefficient of coincidence analysis, with *mnT12* divided into 4 intervals (Figure 3a, Extended Data Figure 4; Extended Data Table 1; Methods). Controls exhibit a robust signature of interference (I): complete interference ($I=1$) for adjacent interval pairs; strong but reduced interference for pairs at intermediate distance; and, high “negative” interference ($I<0$) for the pair of intervals including opposite ends of the chromosome, indicating that a

chromosome with a focus in one end-interval has an increased likelihood of a second focus in the opposite end-interval (Figure 2d top). In contrast, the *syp-1* RNAi data show reduced interference for adjacent interval pairs, and no interference for interval pairs separated by >1 intervals, indicating attenuated interference. Second, we used a gamma distribution to model inter-focus distances (expressed as % of total axis length), and generated best-fit probability density curves where the shape parameter (γ) is a relative indicator of interference strength, with γ=1 indicating no interference and higher values signifying stronger interference[18] (Figure 3b; Extended Data Figure 5). While the control displayed very strong interference (γ=37), *syp-1* RNAi displayed a substantial attenuation of interference (γ=4.9).

A separate analysis of our *mnT12* data yielded another key finding: COSA-1-marked COs are associated with a local increase in chromosome axis length (Figure 4). Plotting the mean axis length for *syp-1* RNAi *mnT12* with 1, 2, 3, or 4 foci revealed a striking linear relationship between number of COSA-1 foci and mean axis length (R^2=0.952), with the slope of the linear regression line indicating that each COSA-1 focus is associated with a 0.4 μm increase in axis length (Figure 4a). Further, association between number of foci and axis length was also observed in controls (Figure 4a). Moreover, comparison of *mnT12* axis lengths in a *spo-11* mutant (which lacks COs) and in *spo-11/+* controls yielded a similar linear relationship for *mnT12* with 0, 1, or 2 COSA-1 foci (Figure 4b; slope=0.49, R^2=0.952). Analysis of unfused autosomes from *spo-11*, controls, and *syp-1* RNAi worms likewise showed each COSA-1 focus associating with a 0.4 μm increase in axis length (Figure 4c; R^2=0.999), demonstrating that the relationship between COs and axis length is generalizable to other chromosomes. Together, these data indicate that extension of chromosome axes occurs in response to CO designation. Finally, assessment of the distance between the left end of the chromosome and the position of the HIM-8 focus on control *mnT12* (Figure 4d; Extended Data Figure 6) revealed that the mean length of this specific short axis segment was increased by 0.4-0.5 μm when a COSA-1 focus was present in the segment. As this value is comparable to that inferred from the linear regression analyses, we conclude that the increase in axis length associated with each CO is predominantly a local effect.

Our demonstration that partial depletion of SYPs attenuates the robust CO interference in *C. elegans* indicates a role for SC central region proteins in CO control. This effect of SYP depletion on interference could reflect a decreased ability to propagate an inhibitory signal, a reduced sensitivity of recombination precursors to inhibition, and/or a prolonged state of competence for CO designation. Our finding that SC central region subunits play a role in achieving the high level of interference characteristic of *C. elegans* meiosis can be reconciled with studies concluding that the SC is dispensable for interference in budding yeast[19-21], based on several considerations. There is a growing body of evidence that at least in some organisms, non-random distribution of prospective CO intermediates may occur in (at least) two different steps[22-24]. This suggests that multiple layers of regulation can contribute to the final interference distribution of COs, raising the possibility that the relative contributions of different CO control mechanisms may differ between organisms. Thus, given that the attenuated interference observed following SYP-1 partial depletion in *C. elegans* (γ=4.9) appears at least as strong or stronger than the interference observed in

wild-type budding yeast (γ=1.9)[25], we suggest that *C. elegans* may utilize a layer of CO control that does not make a significant contribution in budding yeast.

Integrating our findings with prior data showing that CO designation in *C. elegans* occurs in the context of assembled SCs[5,26], we suggest a model in which CO designation requires a capacity for local expansion of previously-assembled meiotic chromosome structures. We suggest that local expansion in turn alters the thickness, density, and/or rigidity of structures beyond the local area, thereby reducing the capacity for axis expansion at other sites (see discussion in Supplementary Information). Overall, our work supports the idea that meiotic CO regulation operates as a self-limiting system in which meiotic chromosome structures create an environment that promotes COs, which in turn modify chromosome structures to inhibit CO formation at additional neighboring sites.

Methods

C. elegans *strains, genetics, and culture conditions*

All strains are from the Bristol N2 background and were maintained and crossed at 20°C under standard conditions. Temperatures used for specific experiments are indicated in Figures and below.

The following strains were used in this study:

AV307: syp-1(me17) V / nT1[unc-?(n754) let-? qIs50] (IV;V).

AV630: *meIs8[unc-119(+) Ppie-1::gfp::cosa-1] II.*

AV647: meIs8[unc-119(+) Ppie-1::gfp::cosa-1] II; spo-11(me44) IV / nT1[unc-?(n754) let-? qIs50] (IV;V).

AV695: meIs8[unc-119(+) Ppie-1::gfp::cosa-1] II; mnT12 (IV;X).

AV760: meIs8[unc-119(+) Ppie-1::gfp::cosa-1] II; unc-24(e138) dpy-4(e1166) mnT12 (IV;X).

AV761: meIs8[unc-119(+) Ppie-1::gfp::cosa-1] II; spo-11(me44) IV / nT1[qIs51] (IV;V).

Additional information on strains:

qIs50 contains *[Pmyo-2::gfp; Ppes-10::gfp; PF22B7.9::gfp]*.

qIs51 contains *[Pmyo-2::gfp; Ppes-10::gfp; PF22B7.9::gfp]*.

For Figure 4b and c and Extended Data Figure 6, *meIs18; spo-11 mnT12* worms (and control *meIs18; spo-11/+ mnT12* worms) were obtained by the following scheme:

1. AV761 males x AV760 hermaphrodites;
2. *meIs18*; + spo-11 + IV / unc-24(e138) + dpy-4(e1166) mnT12 (IV;X) males (from Cross 1) x AV760 hermaphrodites;

3. Progeny from Cross 2 were singly plated. *meIs18*; + spo-11 + mnT12 / unc-24(e138) + dpy-4(e1166) mnT12 (IV;X) hermaphrodites were identified based on failure to produce male self progeny, indicating homozygosity for *mnT12*.

4. From step 3 plates that did not produce male progeny, 20-24 hr post-L4 non-Unc non-Dpy hermaphrodite progeny were used for IF. These included both *spo-11* homozygotes and *spo-11*/+ worms, which were used as controls. *spo-11* mutant and control gonads were dissected onto the same slides and were differentiated during imaging based on DAPI-stained bodies in diakinesis-stage oocytes (10 univalents in *spo-11* oocytes and 5 bivalents in controls).

Experimental conditions for partial depletion of SYP-1 by RNAi

For *syp-1* partial RNAi, synchronized L1 larvae (grown at 20°C from eggs hatched on unseeded plates for 24 hr) were placed on fresh NGM+Amp+IPTG plates recently seeded with *Escherichia coli* HT115 cells containing either a fragment of the *syp-1/F26D2.2* gene in the L4440 vector, or the empty vector (referred to as "control") from the Ahringer Lab RNAi library[28]. For analyses of GFP::COSA-1 foci in late pachytene nuclei, hermaphrodite worms were grown at 25°C starting at the L1 stage and dissected for immunofluorescence (IF) at 16-22 hr post-L4 stage to obtain optimal SYP-1 depletion for observing an increase in GFP::COSA-1 foci; for quantitation of chiasmata, worms were dissected at 24-30 hr post-L4 to permit nuclei with optimal SYP-1 depletion in late pachytene at 16-22 hr post-L4 to progress to diakinesis. Differences in experimental culture conditions (*i.e.* growth at 25°C on *E. coli* HT115 on NGM+Amp+IPTG *vs.* growth at 20°C on *E. coli* OP50 on NGM) likely account for the higher baseline frequency of *mnT12* chromosome pairs with two GFP::COSA-1 foci in the present study (49%) compared to the previous study of Yokoo *et al.* (30%)[5].

Evaluation of SYP-1 partial depletion

RNAi partial depletion conditions used for our experiments were consistently and deliberately much less severe than the level of partial SYP-1 depletion used in the work of Hayashi *et al.*, 2010. Under the conditions used for the current work, the vast majority of pachytene nuclei had assembled SCs on all six chromosome pairs and most diakinesis oocytes had chiasmata connecting all six chromosome pairs (see main text). (In contrast, the vast majority of pachytene nuclei analyzed by Hayashi *et al.* 2010 had assembled SCs on only 1, 2 or 3 chromosome pairs, and in the worms used for their CO analysis, most diakinesis oocytes had multiple achiasmate chromosome pairs[9].) To assess the extent of partial depletion used in the current study, two different approaches were used:

Immunoblotting—The extent of SYP-1 depletion achieved by our RNAi conditions was estimated using Western blot analysis (Extended Data Figure 1a). Protein lysates were generated from control, *syp-1 RNAi*, and *syp-1(me17)* mutant worms (100 worms each; see below). For each experiment, protein blots containing identical amounts of each lysate, plus a dilution series of the control lysate, were probed with α-SYP-1 antibody, and the extent of depletion was estimated by comparing the residual SYP-1 band in the *syp-1* RNAi lysate to the SYP-1 bands in the dilution series from a control lysate processed in parallel.

Protocol details: 100 worms (treated and staged as for the reported IF analyses) were picked to unseeded plates, washed off plates with 1.5 ml of cold M9, and spun down at 2000 rpm for 1 minute. After placing on ice for 1 minute, supernatant was removed, and worm pellets were washed 3× with cold M9 prior to the addition of 2× Laemelli buffer with β-mercaptoethanol (Bio-Rad) and boiling for 10 min to create worm protein lysates. Samples of each lysate were run on a 4-15% Bio-Rad TGX acrylamide gel and then transferred to nitrocellulose membrane using a wet Western blot transfer system (Bio-Rad). Membrane was blocked in 5% milk in 1× TBST for 1 hour at room temperature and then incubated with 1:500 dilution of rabbit α-SYP-1 antibody[12] (pre-absorbed with *syp-1(me17)* dissected worms) in 5% milk in 1× TBST overnight at 4°C. Membrane was washed 5 × 10 min in 1× TBST prior to addition of 1:4000 dilution of goat α-rabbit HRP-conjugated antibody in 5% milk in TBST for 2 hours at room temperature. Following 5 × 10 min washes in 1× TBST, membrane was incubated with Clarity Western ECL substrate (Bio-Rad) for 5 min at room temperature and then exposed to film. To assess loading, antibodies were removed from the membrane with mild stripping buffer (Abcam), and the membrane was then blocked, incubated, and washed as described above except for the following modification for the primary antibody: 1:10,000 mouse α-alpha-tubulin antibody (Sigma #T6199) in 5% milk in TBST, incubated for 1 hr at 4°C.

Fluorescence quantification—For Extended Data Figure 1b-c, normalized fluorescence levels were assessed from IF slides of control and *syp-1* partial RNAi gonads imaged on the DeltaVision microscope using the imaging conditions described below. During image acquisition, exposure times for channels assessing SYP-1 and HTP-3 fluorescence signals were kept the same for both control and *syp-1 RNAi* slides. Deconvolved images were projected using a sum projection algorithm with softWoRx (Applied Precision) software. Using the Edit Polygon tool in softWoRx, individual nuclei from a specific region of the gonad (from 2 rows prior to COSA-1 foci formation, to 3 rows following COSA-1 foci formation) were traced and assessed for SYP-1 and HTP-3 fluorescence intensity. Nuclei were assessed only if they were completely contained within the image stack and did not overlap with any other nuclei in the projected image. (Nuclei with compact DAPI signals indicative of arrest and/or apoptosis were excluded). Further, a subset of *syp-1* RNAi gonads (40%) that exhibited severe SYP-1 depletion (*i.e.* SYP-1 was not detected on all chromosomes) was excluded from this analysis, since gonads in this category would have been excluded from our experiments evaluating numbers and distribution COSA-1 foci based on presence of asynapsed chromosomes and/or inability to trace continuous chromosome axes (as a result of asynapsis).

For each gonad, background fluorescence in the SYP-1 and HTP-3 channels was assessed by measuring fluorescence intensities for three separate areas between nuclei in the scored region and using these to calculate the average background fluorescence per pixel. For each individual nucleus, SYP-1 and HTP-3 fluorescence measurements were calculated by dividing the total intensity by the total area of the projected nucleus, and then subtracting the average background fluorescence for the gonad. To obtain an average SYP-1:HTP-3 ratio for each gonad, the SYP-1:HTP-3 ratios calculated for each nucleus within a given gonad were averaged. Once average SYP-1:HTP-3 ratios were measured for all gonads, two

different approaches were used to compare SYP-1:HTP-3 ratios for *syp-1* RNAi gonads and control gonads:

1. "Mean of Experiments" For each experiment, the average SYP-1:HTP-3 ratios for control gonads and for *syp*-1 RNAi gonads were calculated; the control value was set to 1, and the normalized SYP-1:HTP-3 ratio for *syp-1* RNAi for that particular experiment was expressed as a fraction of the control value. The corresponding graph plots the average normalized SYP-1:HTP-3 ratio for *syp-1* RNAi ± standard deviation for 3 independent experiments.
2. "Mean of all gonads" For each individual experiment, the SYP-1:HTP-3 ratio for each individual gonad (both *syp-1* RNAi and control) was normalized to the average control SYP-1:HTP-3 ratio obtained from the same experiment. These values were then used to calculate average (± standard deviation) normalized SYP-1:HTP-3 ratios for all control gonads and for all *syp-1* RNAi gonads across all experiments. Note that this latter approach makes it possible to convey the variability in the control measurements in the corresponding graph.

Numbers of gonads assessed: Experiment #1 (control = 7 gonads; *syp-1* RNAi = 7 gonads); Experiment #2 (control = 15 gonads; *syp-1* RNAi = 6 gonads); Experiment #3 (control = 10 gonads; *syp-1* RNAi = 8 gonads).

Of the two approaches, the Western blot analysis provides a somewhat lower estimate of residual SYP-1 levels, in part because the subset of worms with more severe SYP-1 depletion (which would have been excluded from our experiments) are included in the protein lysates. Thus, the immunofluorescence approach likely provides a better estimate of the residual SYP-1 levels present in the nuclei analyzed in our experiments.

Since our data indicate that a 60-70% reduction in SYP-1 levels can lead to elevated COSA-1-marked CO sites and impaired interference, we also tested whether the *syp-1* locus might be haplo-insufficient. As we observed 6.02 ± 0.31 (mean ± standard deviation, n=53) and 6.00 ± 0.13 (± standard deviation, n=114) GFP::COSA-1 foci per late pachytene nucleus of *syp-1(me17)/* + and *syp-3(ok758)/*+ worms respectively, we conclude that reducing *syp-1* gene dose by half is not sufficient to impair the robust CO control system.

Immunofluorescence

IFs were performed as described previously[29], with modifications. Gonads from adult worms at 18-24 hr post-L4 stage were dissected. Slides were mounted with Vectashield (except for confocal images, which were mounted with Invitrogen ProLong Gold) and a coverslip with a 170 ± 5 μm thickness. Slides were sealed with nail polish immediately following mounting and stored at 4°C prior to imaging (except for confocal slides which were cured for 24 hr at room temperature prior to sealing and storing at 4°C). All slides were imaged (as described below) within two weeks of preparation. The following primary antibody dilutions were used: rabbit anti-GFP (1:1000)[5]; chicken anti-GFP (1:1000) (Abcam 13970); guinea pig anti-SYP-1 (1:200)[12]; chicken anti-HTP-3 (1:500)[30]; rabbit anti-HIM-3 (1:200)[31]; guinea pig anti-HIM-8 (1:500)[17].

Imaging

For Figure 1, IF slides were imaged at 512 × 512 pixel dimensions on an Applied Precision DeltaVision microscope using a 60× objective with 1.5× optivar. Images were acquired as Z-stacks at 0.2 μm intervals and deconvolved with Applied Precision softWoRx deconvolution software. For Figures 2-4, IF slides were imaged at 1024×1024 pixel dimensions on a Leica SP2 AOBS Confocal microscope using a 63× objective with 4.7× zoom in 12-bit format. Images were acquired as Z-stacks at 81 nm intervals and deconvolved with Huygens Professional deconvolution software (Scientific Volume Imaging). For quantification of GFP::COSA-1 foci, nuclei that were in the last 4-5 rows of late pachytene and were completely contained within the image stack were analyzed. Foci were quantified manually from deconvolved three-dimensional stacks. For visualization and quantitation of chiasmata (Figure 1c and Extended Data Figure 3a), individual *mnT12* bivalents from diakinesis nuclei in −2, −3, or −4 oocytes were identified based on size, cropped, and rotated in three-dimensions using Volocity (PerkinElmer) three-dimensional rendering software. Scoring of chiasmata was based primarily on HTP-3 (chromosome axis) and DAPI staining, as GFP::COSA-1 dissociates from chromosomes during progression through the diakinesis stage. For Figure 1a, images shown are projections through three-dimensional data stacks encompassing whole nuclei, generated with a maximum-intensity algorithm with the softWoRx (Applied Precision) software. For Figure 1c, the images shown are snapshots of a Volocity three-dimensional rendering of individual diakinesis bivalents with maximum intensity rendering for HTP-3. Images shown in Figures 2a and 4c are projections through three-dimensional data stacks encompassing whole nuclei, or straightened chromosomes, generated with a maximum-intensity algorithm using Priism/IVE software[32].

γ-irradiation experiments

L1 progeny from AV647 worms (heterozygous for *spo-11(me44)* and the *nT1* balancer chromosome) were subjected to RNAi conditions described above. *spo-11(me44)* homozygotes were picked at the L4 stage from the RNAi plates based on lack of dominant markers associated with the balancer and placed on freshly seeded RNAi plates at 25°C. At 12 hr post-L4, 25°C *syp-1* and control RNAi-treated worms were γ-irradiated with a Cs-137 source at either 250 Rad, 1000 Rad, 2000 Rad, 4000 Rad, 6000 Rad, or 10,000 Rad. Following γ-irradiation, worms were placed back at 25°C for 8 hr until dissection for IF. Unirradiated controls were kept at 25°C and dissected at the same time as γ-irradiated worms.

Prior to quantitation of COSA-1 foci, we used SYP-1 IF to evaluate the efficacy of SYP-1 partial depletion. In the majority of *syp-1* RNAi gonads (57%), pachytene nuclei had detectable SYP-1 along all six chromosome pairs, but IF signals were reduced in intensity relative to controls and there were some small chromosomal regions that lacked SYP-1; gonads in this category (n = 84) were used for quantitation of COSA-1 foci. Gonads with SYP-1 staining comparable to wild-type (18%) and gonads with more severe SYP-1 depletion (*i.e.* SYP-1 was not detected on all chromosomes, 25%) were excluded from this analysis.

For the quantitation of COSA-1, the numbers of nuclei counted for each γ-irradiation dose are as follows: control RNAi, 0 Rad (n=189), 250 Rad (n=310), 1000 Rad (n=243), 2000 Rad (n=201), 4000 Rad (n=119), 6000 Rad (n=212), 10000 Rad (n=52); *syp-1* partial RNAi, 0 Rad (n=138), 250 Rad (n=170), 1000 Rad (n=278), 2000 Rad (n=278), 4000 Rad (n=195), 6000 Rad (n=280), 10000 Rad (n=345).

Measurements along straightened chromosomes and interference analyses

For quantitative analyses of axis lengths and positions and distributions of COSA-1 foci, *mnT12* chromosomes (identified by HIM-8 binding) and unfused autosomes (from the same nuclei) with continuous and unambiguous chromosome axis staining by either HTP-3 or HIM-3 IF were traced in three-dimensions through the center of the chromosome axis (indicated by strongest staining) and computationally straightened as described before[27]. Using these straightened chromosomes, the lengths of the chromosome axes and the positions of the HIM-8 focus and COSA-1 foci along *mnT12* were measured using Priism/IVE. The left end of the *mnT12* fusion chromosome (identified based on proximity to the HIM-8 focus) was assigned the zero coordinate, and position coordinates (in μm) were determined and recorded for the center of the HIM-8 focus, the centers of each COSA-1 focus, and the opposite end of the chromosome axis. For these analyses, only nuclei in the last 4 rows of late pachytene that were completely contained within the image stacks were analyzed. For the *syp-1* RNAi gonads analyzed, *mnT12* was examined in all nuclei meeting these criteria (115 total *mnT12* chromosomes from 16 gonads, 4 experiments, except for Figures 2d-e and 3, where six *mnT12* chromosomes were omitted from the analyses due to lack of positional information for proper interval binning). For control analyses where the relative frequencies of *mnT12* chromosomes with 1 vs. 2 COSA-1 foci were a relevant factor (Figures 2b, 3a, 4a left, and Extended Data Figure 4), we similarly used data from gonads where all nuclei meeting the above-specified criteria were included (69 *mnT12* chromosomes from 6 gonads, 3 experiments, except for Figure 3a, where one *mnT12* chromosome was omitted from the analyses due to lack of positional information for proper interval binning). For Figures 2c-e, 3b, and 4d, 16 additional control *mnT12* chromosomes with 2 COSA-1 foci from 2 additional gonads were also included in the analyses. Numbers for Figure 4b: *spo-11*/+ control (93 *mnT12* chromosomes from 13 gonads, 5 experiments); *spo-11* (75 *mnT12* chromosomes from 7 gonads, 3 experiments). For Extended Data Figure 6, data from the same nuclei, plus 20 additional *mnT12* control chromosomes with HIM-8 positional data (from 5 gonads), were included in the analysis. The best-fit linear regression lines in Figure 4a-b (and corresponding R^2 values) were generated by the Prism graphing program (GraphPad Software). For Figures 2d, 2e and Extended Data Figure 4, positions of foci were normalized by dividing each chromosome into 8 intervals of equal size and binning the foci into these 8 intervals.

For the interference strength analysis in Figure 3a, positions of foci were normalized by dividing each chromosome into 4 intervals of equal size and binning the foci into these 4 intervals. For each specified pair of intervals tested, this coefficient of coincidence analysis compared the observed frequency of COSA-1 foci occurring in both intervals with the frequency expected if foci occurred independently in the two intervals (*i.e.* absence of interference), with Interference Strength (I) calculated as (1 – observed/expected). The

"expected" number of chromosomes with COSA-1 foci occurring in both of a given pair of intervals (X and Y) was calculated as: [measured frequency of COSA-1 foci in interval X] × [measured frequency of COSA-1 foci in interval Y] × [number of *mnT12* chromosomes examined].

For determining interference strength using the best-fit gamma distribution analyses in Figure 3b and Extended Data Figure 5, distances between COSA-1 foci along straightened *mnT12* chromosomes were normalized by calculating the percent axis length separating neighboring COSA-1 foci. Distances between adjacent foci expressed as percent axis length were entered into the EasyFit Distribution Fitting Software (Mathwave) to generate histograms of the data sets and best-fit probability distribution curves. Numbers of inter-focus distances used are: control (n=47); *syp-1* RNAi (n=183).

In addition to measuring *mnT12* axis lengths, we also measured axis lengths of unfused autosomes with continuous and unambiguous HTP-3 or HIM-3 staining from the same nuclei used to measure *mnT12.* Numbers of chromosomes analyzed were: controls at 25°C (208 autosomes from 62 nuclei, 6 gonads, 3 experiments); *syp-1* RNAi at 25°C (155 autosomes from 58 nuclei, 16 gonads, 4 experiments); *spo-11/+* controls at 20°C (233 autosomes from 77 nuclei, 13 gonads, 5 experiments); and *spo-11* at 20°C (203 autosomes from 62 nuclei, 7 gonads, 3 experiments). As mean axis lengths of unfused autosomes in RNAi controls at 25°C and *spo-11/+* controls at 20°C were nearly identical (6.42 ± 0.06 μm vs. 6.46 ± 0.04 μm; ± s.e.m.), these two data sets were combined to give a single control value for the graph in Figure 4c.

Statistics

All p-values reported in the main text and Extended Data Figures 2 and 6 are two-tailed and calculated from Mann-Whitney tests, which are robust non-parametric statistical tests appropriate for the relevant data sets. For the 4-interval data set analysis in Figure 3a, we used Fisher's exact test (an appropriate test for 2×2 contingency tables) to evaluate (for each pair of intervals) whether COSA-1 foci occurred independently in the two intervals under consideration (Extended Data Table 1). For the two-tailed p-value reported in Extended Data Figure 3b comparing the observed vs. expected outcome for GFP::COSA-1 foci within an asynapsed region of the *mnT12* chromosome for *syp-1* RNAi, the χ^2 test was utilized as it is an appropriate test to compare observed vs. expected outcomes for categorical data. For Figures 4a-c, the goodness-of-fit for the linear regression lines were reported as coefficient of determination (R^2; an appropriate goodness-of-fit statistic for fitted linear regression lines), using the Prism graphing program (GraphPad Software). For all tests described above, the assumptions of each test were met.

Supplementary Material

Refer to Web version on PubMed Central for supplementary material.

Acknowledgements

We thank A. Dernburg and M. Zetka for antibodies and the CGC (funded by NIH P40 OD010440) for strains. We thank K. Hillers and K. Zawadzki for helpful comments on the manuscript. This work was supported by a Helen

Hay Whitney Foundation Postdoctoral Fellowship, a Katharine McCormick Advanced Postdoctoral Fellowship, and NIH K99 HD07616501 to DEL and by NIH R01 GM067268 to AMV. BJM is an investigator of the Howard Hughes Medical Institute.

References

1. Page SL, Hawley RS. Chromosome choreography: the meiotic ballet. Science. 2003; 301:785–789. [PubMed: 12907787]
2. Martinez-Perez E, Colaiacovo MP. Distribution of meiotic recombination events: talking to your neighbors. Curr. Opin. Genet. Dev. 2009; 19:105–112. [PubMed: 19328674]
3. Muller HJ. The mechanism of crossing-over. Am. Naturalist. 1916; 50:193–221.
4. Sturtevant AH. The linear arrangements of six sex-linked factors in *Drosophila*, as shown by their mode of association. J. Exp. Zoology. 1913; 14:43–59.
5. Yokoo R, et al. COSA-1 reveals robust homeostasis and separable licensing and reinforcement steps governing meiotic crossovers. Cell. 2012; 149:75–87. [PubMed: 22464324]
6. Bishop DK, Zickler D. Early decision; meiotic crossover interference prior to stable strand exchange and synapsis. Cell. 2004; 117:9–15. [PubMed: 15066278]
7. Egel R. Synaptonemal complex and crossing-over: structural support or interference? Heredity (Edinb). 1978; 41:233–237. [PubMed: 282284]
8. Maguire MP. Can abortive early homologous associations promote increased crossing-over in an adjacent rearranged segment? Genome. 1988; 30:469–472. [PubMed: 3209058]
9. Hayashi M, Mlynarczyk-Evans S, Villeneuve AM. The synaptonemal complex shapes the crossover landscape through cooperative assembly, crossover promotion and crossover inhibition during *Caenorhabditis elegans* meiosis. Genetics. 2010; 186:45–58. [PubMed: 20592266]
10. Hillers KJ, Villeneuve AM. Chromosome-wide control of meiotic crossing over in *C. elegans*. Curr. Biol. 2003; 13:1641–1647. [PubMed: 13678597]
11. Colaiacovo MP, et al. Synaptonemal complex assembly in *C. elegans* is dispensable for loading strand-exchange proteins but critical for proper completion of recombination. Dev. Cell. 2003; 5:463–474. [PubMed: 12967565]
12. MacQueen AJ, Colaiacovo MP, McDonald K, Villeneuve AM. Synapsis-dependent and -independent mechanisms stabilize homolog pairing during meiotic prophase in *C. elegans*. Genes Dev. 2002; 16:2428–2442. [PubMed: 12231631]
13. Smolikov S, et al. SYP-3 restricts synaptonemal complex assembly to bridge paired chromosome axes during meiosis in *Caenorhabditis elegans*. Genetics. 2007; 176:2015–2025. [PubMed: 17565948]
14. Dernburg AF, et al. Meiotic recombination in *C. elegans* initiates by a conserved mechanism and is dispensable for homologous chromosome synapsis. Cell. 1998; 94:387–398. [PubMed: 9708740]
15. Sigurdson DC, Herman RK, Horton CA, Kari CK, Pratt SE. An X-autosome fusion chromosome of *Caenorhabditis elegans*. Mol. Gen. Genet. 1986; 202:212–218. [PubMed: 3458021]
16. Goodyer W, et al. HTP-3 links DSB formation with homolog pairing and crossing over during *C. elegans* meiosis. Dev. Cell. 2008; 14:263–274. [PubMed: 18267094]
17. Phillips CM, et al. HIM-8 binds to the X chromosome pairing center and mediates chromosome-specific meiotic synapsis. Cell. 2005; 123:1051–1063. [PubMed: 16360035]
18. McPeek MS, Speed TP. Modeling interference in genetic recombination. Genetics. 1995; 139:1031–1044. [PubMed: 7713406]
19. Fung JC, Rockmill B, Odell M, Roeder GS. Imposition of crossover interference through the nonrandom distribution of synapsis initiation complexes. Cell. 2004; 116:795–802. [PubMed: 15035982]
20. Borner GV, Kleckner N, Hunter N. Crossover/noncrossover differentiation, synaptonemal complex formation, and regulatory surveillance at the leptotene/zygotene transition of meiosis. Cell. 2004; 117:29–45. [PubMed: 15066280]
21. Storlazzi A, Xu L, Schwacha A, Kleckner N. Synaptonemal complex (SC) component Zip1 plays a role in meiotic recombination independent of SC polymerization along the chromosomes. Proc. Natl Acad. Sci. USA. 1996; 93:9043–9048. [PubMed: 8799151]

22. Cole F, et al. Homeostatic control of recombination is implemented progressively in mouse meiosis. Nature Cell Biol. 2012; 14:424–430. [PubMed: 22388890]
23. de Boer E, Stam P, Dietrich AJ, Pastink A, Heyting C. Two levels of interference in mouse meiotic recombination. Proc. Natl Acad. Sci. USA. 2006; 103:9607–9612. [PubMed: 16766662]
24. Reynolds A, et al. RNF212 is a dosage-sensitive regulator of crossing-over during mammalian meiosis. Nature Genet. 2013; 45:269–278. [PubMed: 23396135]
25. Chen SY, et al. Global analysis of the meiotic crossover landscape. Dev. Cell. 2008; 15:401–415. [PubMed: 18691940]
26. Rosu S, Libuda DE, Villeneuve AM. Robust crossover assurance and regulated interhomolog access maintain meiotic crossover number. Science. 2011; 334:1286–1289. [PubMed: 22144627]
27. Mets DG, Meyer BJ. Condensins regulate meiotic DNA break distribution, thus crossover frequency, by controlling chromosome structure. Cell. 2009; 139:73–86. [PubMed: 19781752]
28. Kamath RS, et al. Systematic functional analysis of the *Caenorhabditis elegans* genome using RNAi. Nature. 2003; 421:231–237. [PubMed: 12529635]
29. Martinez-Perez E, Villeneuve AM. HTP-1-dependent constraints coordinate homolog pairing and synapsis and promote chiasma formation during *C. elegans* meiosis. Genes Dev. 2005; 19:2727–2743. [PubMed: 16291646]
30. MacQueen AJ, et al. Chromosome sites play dual roles to establish homologous synapsis during meiosis in *C. elegans*. Cell. 2005; 123:1037–1050. [PubMed: 16360034]
31. Zetka MC, Kawasaki I, Strome S, Muller F. Synapsis and chiasma formation in Caenorhabditis elegans require HIM-3, a meiotic chromosome core component that functions in chromosome segregation. Genes Dev. 1999; 13:2258–2270. [PubMed: 10485848]
32. Chen H, Hughes DD, Chan TA, Sedat JW, Agard DA. IVE (Image Visualization Environment): a software platform for all three-dimensional microscopy applications. J. Struct. Biol. 1996; 116:56–60. doi:10.1006/jsbi.1996.0010. [PubMed: 8742723]

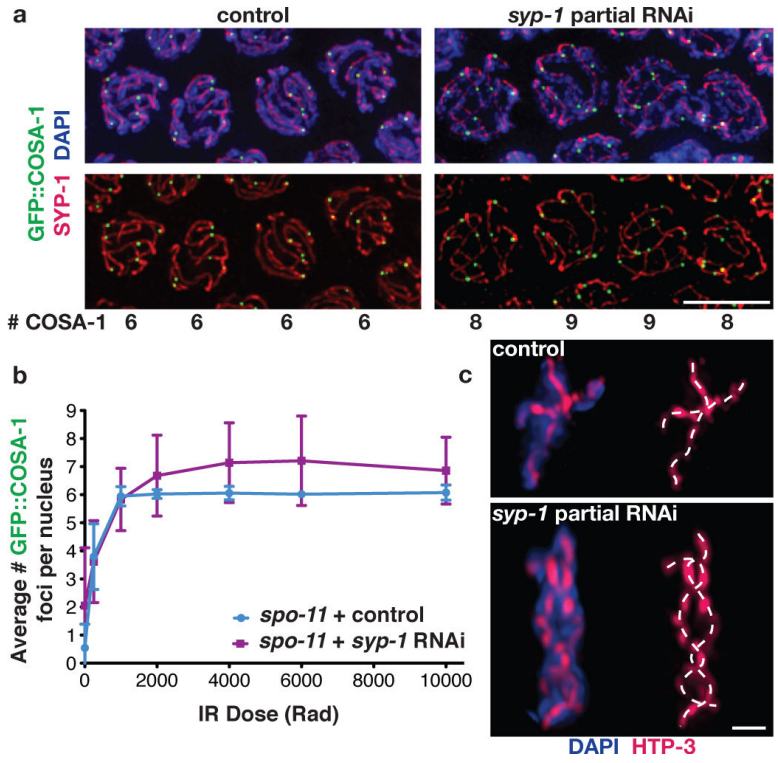

Figure 1. SYP-1 partial depletion increases numbers of COSA-1 foci and chiasmata

(a) Immunofluorescence (IF) images of late pachytene nuclei from control or *syp-1* partial RNAi worms. Scale bar represents 5 μm. **(b)** Dose-response graph depicting mean numbers of GFP::COSA-1 foci formed per nucleus in response to DSBs generated by increasing doses of γ-irradiation (Rad). See Methods for numbers of nuclei used; error bars indicate s.d. At >1000 Rad, both the mean numbers of foci and s.d. were increased in *syp-1* RNAi relative to control. **(c)** Three-dimensionally rendered images of individual diakinesis bivalents comprising the *mnT12 (X;IV)* fusion chromosome pair. Dashed lines (white) indicate traced HTP-3 axes, with crossing of axes indicating chiasmata. Scale bar represents 1 μm.

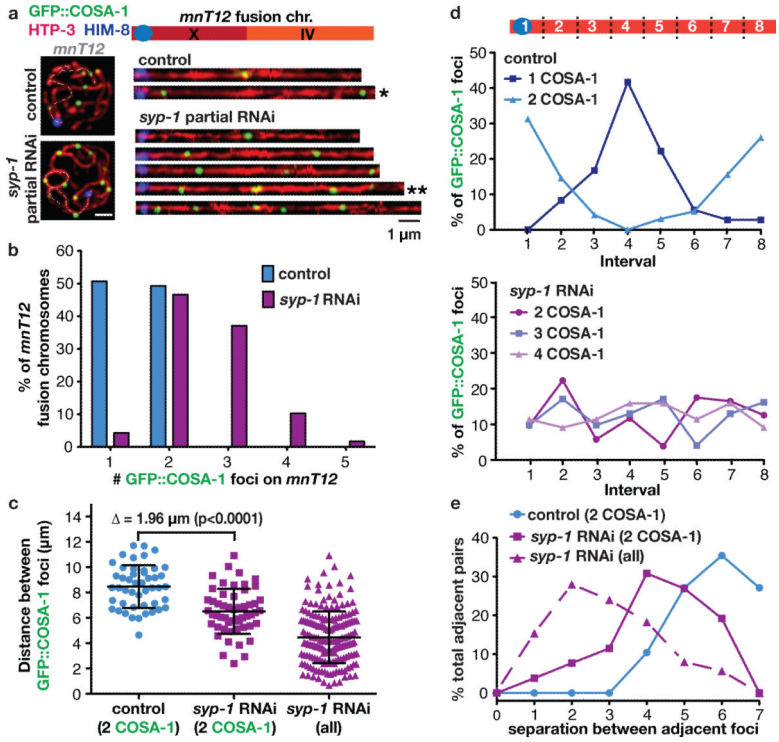

Figure 2. SYP-1 partial depletion attenuates crossover interference

(a) Left images, projections of individual late pachytene nuclei containing the *mnT12* fusion chromosome (depicted schematically at top right), which is identified by its associated HIM-8 focus; gray dotted line indicates the traced three-dimensional path of the *mnT12* chromosome axis. Right images, representative computationally straightened *mnT12* used for quantitative analyses in be and Figures 3-4. *, ** indicate the straightened chromosomes from the nuclei shown. Scale bars indicate 1 µm. **(b)** Graph indicating the percent of *mnT12* with the indicated number of COSA-1 foci for control (n= 69) and *syp-1* RNAi (n=115). **(c)** Scatterplot showing measured distances (µm) between COSA-1 foci on control *mnT12* with 2 foci, on *syp-1* RNAi *mnT12* with 2 foci, and on all *syp-1* RNAi *mnT12* with multiple foci. Horizontal lines indicate the mean; error bars indicate s.d. **(d)** Graphs indicating the distributions of foci among 8 evenly-spaced intervals along the *mnT12* axis (schematic at top) for the subsets of control (top graph) and *syp-1* RNAi (bottom graph) *mnT12* with the indicated numbers of COSA-1 foci. **(e)** Graph depicting the distributions of spacing between adjacent pairs of foci. Using the same 8-interval scheme as in (d), separation values are defined as the number of interval boundaries crossed before encountering the next focus (*i.e.* adjacent foci within the same interval on the same chromosome pair have a separation of 0, adjacent foci in consecutive intervals have a separation of 1, etc.). See Methods for numbers of *mnT12* chromosomes used for (**c**-**e**).

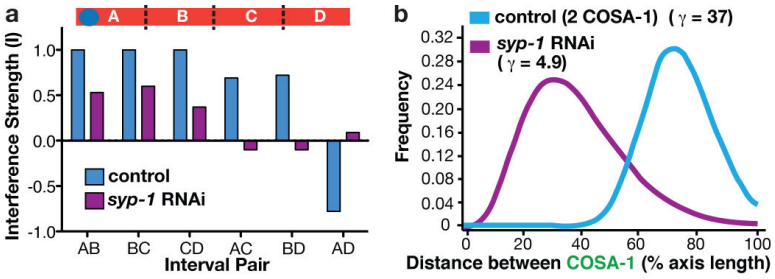

Figure 3. SYP-1 partial depletion decreases crossover interference strength

(a) Graph of Interference strength (I) values for the indicated interval pairs, where I = 1-observed/expected (Methods); schematic (top) indicates division of *mnT12* into 4 intervals for this analysis. **(b)** Graph showing best-fit probability density function curves generated when a gamma distribution was used to model the distribution of inter-focus distances; for this analysis, distances between adjacent foci were expressed as percent of axis length. See Methods for numbers of chromosomes used.

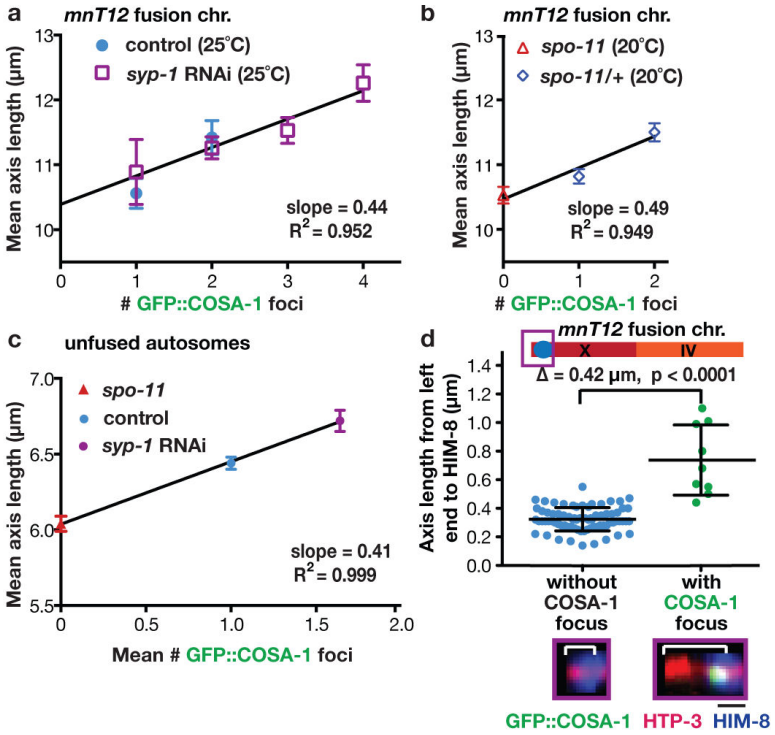

Figure 4. Crossover designation causes a local expansion of chromosome axis length

(a,b) Graphs plotting the relationship between number of COSA-1 foci and mean length (±s.e.m.) of the *mnT12* chromosome axis. **(a)** Data for *syp-1* RNAi and control at 25°C; extrapolated linear regression line was generated using the *syp-1* RNAi data. **(b)** Data for *spo-11* and *spo-11/+* control at 20°C. **(c)** Graph plotting the relationship between mean number of COSA-1 foci and mean axis length (± s.e.m.) for unfused autosomes in *spo-11*, control, and *syp-1* RNAi nuclei (Methods). **(d)** Scatterplot showing length measurements (from control nuclei at 25°C) for the axis segment extending from left end of *mnT12* to the center of the HIM-8 focus for chromosomes that either lacked or had a COSA-1 focus in this segment, as depicted in images below the graph. Horizontal lines indicate mean; error bars indicate s.d. See Methods for numbers of chromosomes used.